Fabrication and Characterization of Supercapacitors toward Self-Powered System

Ananthakumar Ramadoss,
Balasubramaniam Saravanakumar and
Sang-Jae Kim

Additional information is available at the end of the chapter

Abstract

Ever increasing energy demand urges to impelled extensive research in the development of new eco-friendly energy harvesting and storage technologies. Energy harvesting technology exploiting renewable energy sources is an auspicious method for sustainable, autonomous, and everlasting operation of a variety of electronic devices. A new concept of an integrated self-powered system by combining an energy harvesting device with an energy storage device has been established to harvest renewable energy and simultaneously store it for sustainable operation of electronic devices. In this chapter, describes the fabrication of a self-powered system by integrating the supercapacitor with energy harvesting devices such as nanogenerator and solar cells to power portable electronic devices. Initially synthesis and electrochemical characterization of various electroactive materials for supercapacitors and further, fabrication of supercapacitor device were discussed. In conclusion, this chapter demonstrates self-powered system by the integration of energy harvesting, energy storage module with portable electronic devices. The various result validates the feasibility of using supercapacitors as efficient energy storage components in self-powered devices. The proposed self-powered technology based on energy conversion of renewable energy to electrical energy which stored in energy storage device and it will be used to operate several electronic devices as a self-powered device.

Keywords: energy harvesting, energy storage, supercapacitors, self-powered system, portable electronics

1. Introduction

Recently, a massive demand on the highly reliable energy sources with higher energy density and longer life to operate advanced electronic and optoelectronic devices, which have impelled extensive research in the development of new eco-friendly energy harvesting and storage technologies [1–5]. The advancement of portable electronics, enormous demand for electric vehicles, integration, and development of internet of things (IoT) was highly demanding the high-performance energy storage device with added functionalities like flexibility, light-weight, cost-effective, renewable, and eco-friendly features [6, 7]. At the same time, the ultimatum of our society is also looking for an advanced version of multifunctional electronic devices, which are swelling day by day towards the trend of being a portable, flexible, light-weight, wearable and self-powered devices.

In fact, there is a increasing interest in the energy generation from environment for powering the micro/nano-systems, because it is available everywhere and abundant. However, limited by time, location, weather and other factors [8, 9]. For example, solar and wind energies are intermittent energy but renewable. But, we will not get sunshine during the night time and as well as wind on our demand, which results instability or unsustainable power supply to electronic devices [10, 11]. In order to alleviate these problems, renewable energy converters like solar and vibrational harvesters would be better choice to integrate with energy storage device, to achieve sustainable operation by storing the generated electric energy from energy harvesting devices. The nanogenerator is a device which can efficiently convert mechanical energy into electrical energy through piezoelectric and triboelectrification processes from our living/working environment. However, these mechanical energy sources are uncontrollable fluctuation which reflects in output power [11–13]. Therefore, it cannot be used directly to power electronic devices. In this circumstance, an intermediate efficient energy storage system required to store this irregular renewable energy to achieve independent power source (stable and durable output). The development of self-powered micro/nano-device by integrating energy harvesting device with electrochemical energy storage devices such as supercapacitor and battery is a promising solution for the limitation of both energy harvesting and storage devices. Among them, supercapacitors are superior than lithium-ion batteries because of its higher power capacity, more extended cyclic stability, and fast charging/discharging capability, environmental benignancy, etc. [10, 14–16].

Recently, researchers have been attempted to develop a new hybrid system by integrating the energy harvesting device (solar cell and nanogenerator) along with a storage device (lithium-ion battery and supercapacitor) to perform a self-powered operation [8, 17–23]. However, the obtained results are not up to real-world application level due to low energy conversion and storage efficiency of the devices as well as power management circuit, and further research is required to improve the output performance. The performance of self-powered systems will be substantially improved with a better power management circuit and a rational design of energy harvesting and storage devices. In recent years, significant endeavors have been dedicated to building an integrated sustainable self-power system for the smart electronics with the improved architecture of energy harvesting and storage devices.

This chapter describes the fabrication and electrochemical performance of the supercapacitor device with various electrode materials and integration of supercapacitor device with

different energy harvesters such as solar, vibration for self-powered device applications. Briefly, (i) fabrication and integration of supercapacitor device with vibrational energy harvesters such as piezoelectric and triboelectric nanogenerator and (ii) fabrication and integration of supercapacitor device with solar energy harvesters such as a dye-sensitized solar cell (DSSC).

2. Fabrication and testing of self-powered systems

2.1. Fabrication and integration of supercapacitor device with vibrational energy harvesters

Recently, a higher attention has been given to the development of two dimensional (2D) materials for various application such as electronic, catalytic, energy conversion and storage application due to their exceptional property like electrical, optical and chemical properties. Among the other 2D materials, graphene offered higher electrical conductivity, surface area (2600 $m^2 g^{-1}$), and excellent mechanical flexibility due to their excellent physio-chemical properties by honeycomb structured carbon atom with atomic thick [24–28]. Because of higher surface area and good conductivity of graphene attracts to energy storage application. However, the specific capacitance, energy and power density of the graphene supercapacitors are lower than the expected values, which varies with synthesis methods. Until now, a various method has been adapted for synthesis of graphene in different forms like pristine graphene, graphene, reduced graphene oxide (rGO), and graphitic oxides by micromechanical exfoliation from graphite, chemical vapor deposition, chemical reduction methods [29–34]. Herein, a flexible graphene-coated fabric electrodes were fabricated by using a simple-cost effective dip-coating technique followed by thermal reduction at 170°C in Ar for 2 h. This fabrication method allows making binder-free, highly flexible, lightweight supercapacitor device and fabrication process is very simple, cost-effective and possible to extend large scale fabrication. A thin, binder-free coating of graphene allows higher electrical conductivity, surface area, and electrochemical activity.

2.1.1. Fabrication and characterization of the thermally reduced graphene oxide (TRGO)-coated fabric electrode

The fabrication of thermally reduced graphene oxide nanosheets electrode is schematically represented in **Figure 1a**. Briefly, the graphene oxide (GO) was prepared from graphite by modified hummer's method [35]. The prepared GO solution was used to coat on conducting fabric by repeated dip-coating. After each coating, the GO-coated fabric was dried at 60°C for 30 min; this process was repeated for five times. The GO-coated fabric was reduced to a graphene-coated fabric by thermal treatment at 170°C for 2 h in Ar. The surface morphology of the as-prepared film was characterized through Field emission scanning electron microscopy (FE-SEM) analysis, and results are indicating that the uniform deposition of TRGO on the fabric surface which is noted in **Figure 1b–c**. Further, the chemical reduction of GO deposited fabrics was confirmed through Raman, Fourier transforms infrared (FT-IR), and X-ray photoelectron spectroscopy (XPS) analysis and results are presented in **Figure 2**. From Raman spectra (**Figure 2a**), two characteristic peaks were observed at 1602 (G-band) and 1354 cm^{-1}
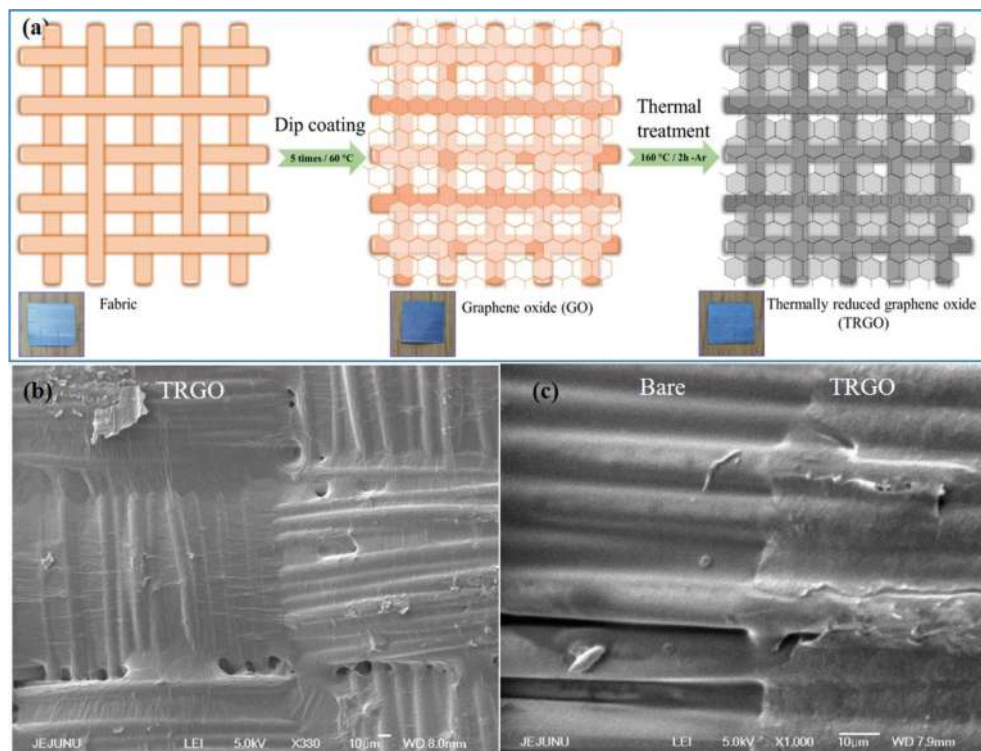
Figure 1. (a) Schematic diagram of the formation of thermally reduced graphene oxide nanosheets. (b-c) FE-SEM images of TRGO on the fabric surface. Figures are reproduced with permission from Ref. [19]. Copyright of Elsevier.

(D-band) of graphitic carbon in both GO and TRGO and corresponds to the defects and disorder in the hexagonal graphitic layers and optical E_{2g} mode in-plane vibration phonon at the Brillouin zone center, respectively [26, 36, 37]. Moreover, the chemical reduction of GO into TRGO by characteristics peak shift toward lower wave number and a slight increase in I_D/I_G ratio from 0.95 to 0.97, it is due to structural disorder (defects) generated during thermal reduction process [33]. The FT-IR spectra (**Figure 2b**.) also clearly indicating the reduction of GO into TRGO through the observation of reduced intensities of the absorption bands at 3340 (O—H stretching vibration), 1728 (C=O stretching vibration), 1623 (skeletal vibration of un-oxidized graphitic domains), 1386 (O—H deformation of C—OH groups), 1233 (C—OH stretching vibration), and 1057 cm^{-1} (C—O stretching vibration) [38]. In XPS spectra, three peaks were observed at 284.6, 286.4, and 288.6 eV, which correspond to C=C/C—C (aromatic rings), C—O (hydroxyl and epoxy), and C=O (carbonyl) groups, respectively [26, 36]. The peak intensities of the oxygen-containing groups in the TRGO was lower than GO due to thermal reduction (**Figure 2c–d**). From, these results concluded that the GO was reduced to TRGO after thermal treatment in Ar environment. Moreover, thermal treatment allowed to transform sp^3 to sp^2 hybridization by reduction of the oxygenating functional group [39].
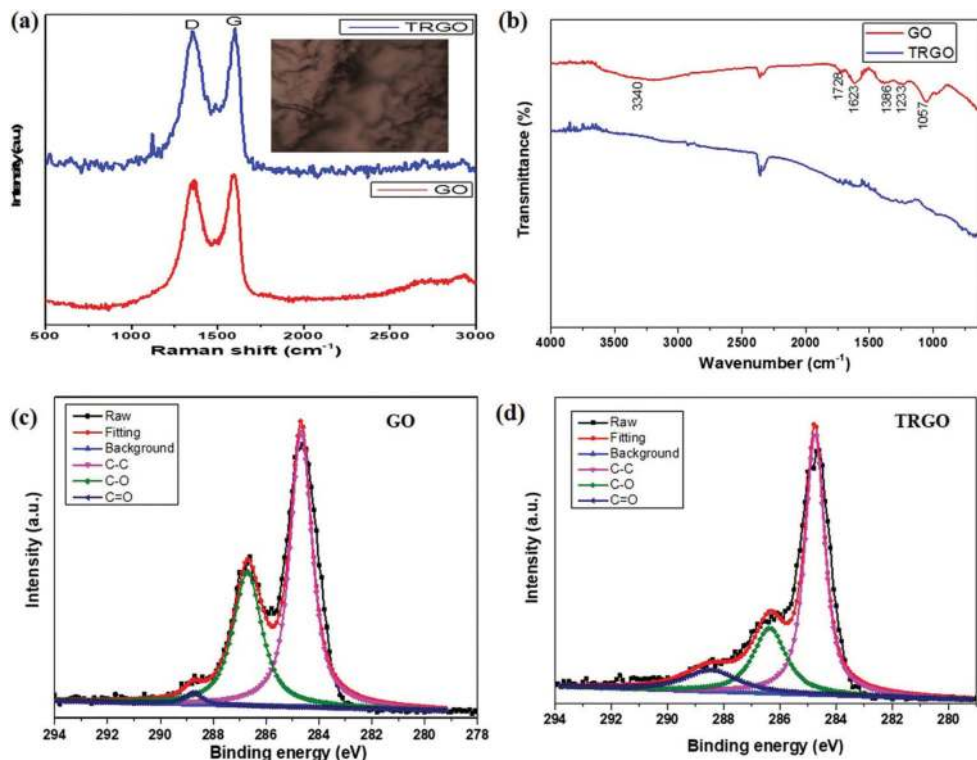
Figure 2. (a) Raman, (b) FT-IR and (c-d) C1s XPS spectra of GO and TRGO. Figures are reproduced with permission from Ref. [19]. Copyright of Elsevier.

2.1.2. Electrochemical characterization of TRGO-coated fabric electrode

The electrochemical performance of the as-prepared TRGO-coated fabric electrode was measured in 1 M H_3PO_4 electrolyte using the three-electrode system. **Figure 3a** shows the cyclic voltammetry (CV) curves of the TRGO-coated fabric electrode at various sweep rates from 5 to 125 mV s^{-1}. The resultant CV curve shows a rectangular-like shape, which indicates the electrochemical double-layer capacitance. Further, the rectangular CV curve accompanied with redox peaks at ~0.32 V of anodic scan and ~0.29 V of the cathodic scan. The co-existence of redox peaks confirmed the Faradic reaction by oxygenated functional groups (carbonyl and quinone groups) in TRGO [36, 40–42], which significantly contributes pseudocapacitance to the system (Inset of **Figure 3a**). The calculated specific capacitance at various scan rates was shown in **Figure 3b**. At a scan rate of 5 mV s^{-1}, the higher specific capacitance of 414 F g^{-1} was observed and drops with increasing scan rates [43]. Further, galvanostatic charge-discharge (GCD) was measured at different current densities and results are shown in **Figure 3c**. The resultant GCD curve shows a linear and symmetric shape with a significantly low plateau. The symmetric nature of GCD confirms the double-layer capacitive nature and small plateau
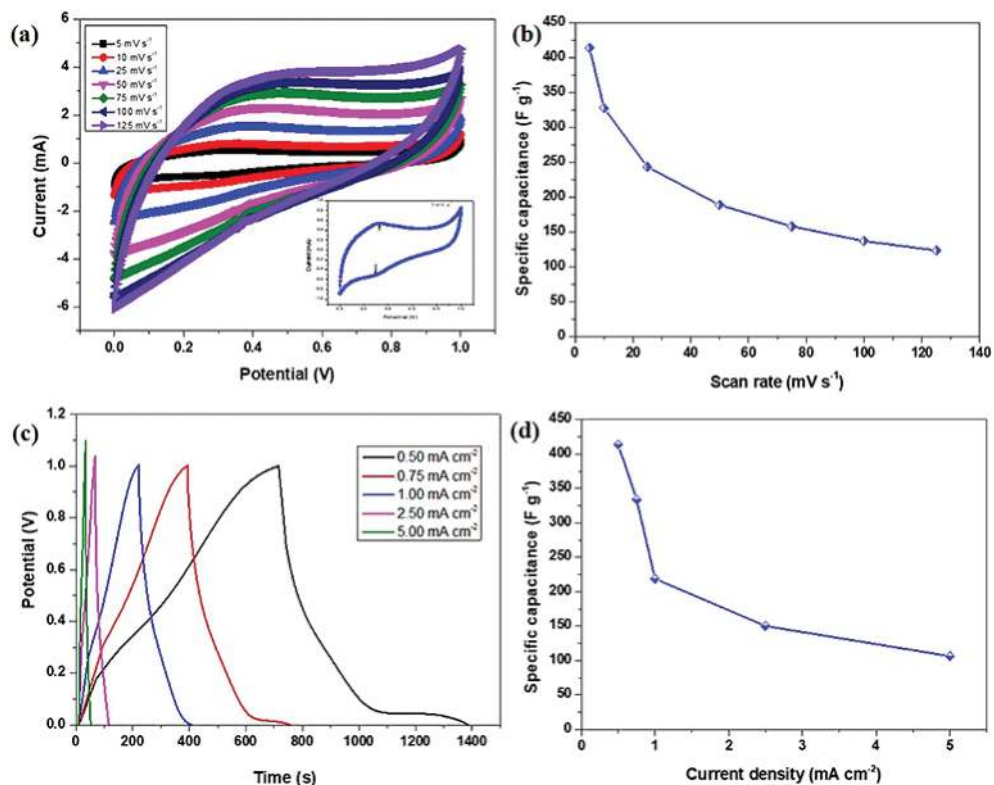
Figure 3. (a) CV curves of TRGO-coated fabric electrodes (inset at 5 mV s^{-1}). (b) Specific capacitance of TRGO-coated fabrics at different scan rates. (c) GCD curves of TRGO-coated fabric electrodes. (d) Specific capacitance of TRGO-coated fabrics at different current densities. Figures are reproduced with permission from Ref. [19]. Copyright of Elsevier.

appeared due to the faradic reaction. The existence of redox peak in GCD curve well agrees with CV curve. The calculated specific capacitances (**Figure 3d**) were 413, 333, 218, 150, and 106 F g^{-1} at various current densities of 0.5, 0.75, 1, 2.5 and 5 mA cm^{-2}, respectively. These values are comparable as well as higher than previously reported values [26, 36, 44–47]. The shorter diffusion path, higher conductivity and higher active surface area of the fabricated TRGO electrode enhances the specific capacitance.

2.1.3. Fabrication and electrochemical performance of the flexible solid-state symmetric supercapacitor (SSC) device

A solid-state SSC was fabricated by sandwiching a H$_3$PO$_4$/PVA gel electrolyte and filter paper between two pieces of the TRGO-coated fabric electrodes. The electrochemical performance of the solid-state supercapacitor such as CV and GCD was measured at different scan rates and current densities and results shown in **Figure 4**. The CV curve (**Figure 4a**.) of the fabricated supercapacitor device showed rectangular-like shapes even at high scan rates, which is ideal capacitive and fast charge/discharge behavior of the supercapacitor device. The
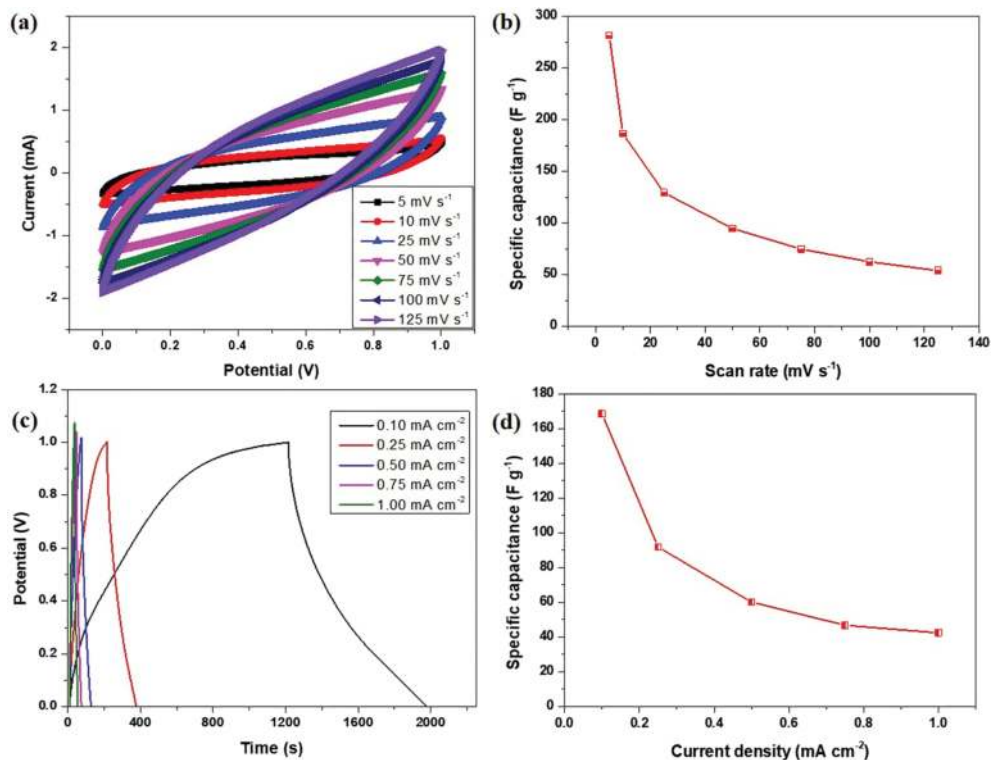
Figure 4. (a) CV curves and (b) specific capacitance of fabric SC at different scan rates. (c) GCD profiles and (d) specific capacitance of fabric SC at current densities. Reproduced from Ref. [19] with permission from the Elsevier.

specific capacitance as a function of scan rate is shown in **Figure 4b**. The calculated single electrode specific capacitance decreased from 281 to 54 F g^{-1}, when scan rate increased from 5 to 125 mV s^{-1} and it is due to inefficient diffusion of ions at higher scan rates [48, 49]. Further, GCD of solid-state device was measured at various current density, which is shown in **Figure 4c**. The resultant GCD curve shows symmetric nature, which confirms the good capacitive nature of the device. The calculated specific capacitance was shown in **Figure 4d**. The estimated specific capacitance of the cell (flexible supercapacitor) was 70.4 F g^{-1} at 5 mV s^{-1}. The highest specific capacitance (single electrode) of 169 F g^{-1} was achieved at a current density of 0.1 mA cm^{-2}; this value is comparable to those previously reported results for solid-state supercapacitors [45, 50, 51]. Further, the power and energy densities are two significant parameters to evaluate the performance of the supercapacitor device. The maximum energy and power densities of the solid-state device reached 5.8 W h kg^{-1} at a power density of 27.7 kW kg^{-1} and a power density of 277.6 kW kg^{-1} at an energy density of 1.5 W h kg^{-1}. The obtained values are higher and comparable to the previously reported values [44, 50, 52–60]. The excellent electrochemical performance of the solid-state SSC device mainly attributed to the following factors: (1) binder-free deposition of graphene on fabric current collector reduces the conduct resistance, which facilitates faster electrical conduction during electrochemical reaction; (2) the

deposition of thin TRGO nanosheets provides a large accessible surface area which allowed abundant ions access (adsorption/desorption) for electrochemical reaction; (3) direct deposition of electroactive material allows strong adhesion with fabric current collector provide higher mechanical flexibility to device.

2.1.4. Integration and functional characterization of self-powered UV sensor

To demonstrate the self-powered application, fabricated SSC device was integrated with piezoelectric nanogenerator and photosensor. Here, piezoelectric nanogenerator used as an energy harvester, which converts the mechanical vibration, environmental noises into electrical energy. The harvested alternate current (AC) electrical signal was stored in the fabricated SSC device with the help of rectifier. The stored energy was used to monitor the ultraviolet (UV) light by integrating the photosensor with this system. The detailed circuit configuration was presented in **Figure 5a**. Here, a commercial piezoelectric nanogenerator was used as the energy source; it generated an average open-circuit voltage and short-circuit current of 8 V and 20 μA, respectively, under continuous finger pressure. The serially connected supercapacitors were charged (0.3 V over 280 s) by piezoelectric nanogenerator under constant finger pressing (**Figure 5b**). To demonstrate a self-powered application, the photodetector was connected to the supercapacitor to monitor UV light (**Figure 5a**) by closing switch S2 and opening switch S1. Here, photodetector was powered by serially connected supercapacitor and photodetector act as a variable load resistance for supercapacitor. The resistance of the photodetector varied linearly with the incident light intensity. The change of load resistance considerably changes the discharge current. The stability of the self-powered device is measured by multiple ON/OFF cycles under a constant illumination intensity of 8 mW cm^{-2} at a wavelength of 365 nm and results showed a stable response during measurement (**Figure 5c**). Additionally, the photoresponse was measured at 0.8 mW cm^{-2} steps for incident light intensity ranging from 0.8 to 8 mW cm^{-2} (**Figure 5d**). The photoresponse current was calculated using the following relation [61]:

$$\left| I_{PR} \right| = \left(I_{OFF} - I_{ON} \right) \tag{1}$$

where, I_{PR} is the photoresponse current, I_{OFF} is the discharge current at UV light "off" condition, and I_{ON} is the discharge current at UV light "on" condition. The photoresponse current increased linearly with increasing incident intensity (**Figure 5e**). This study suggested that the self-powered device has a massive potential in wearable and portable device applications.

2.2. Fabrication and electrochemical characterization of flexible transparent supercapacitor device

First, silver nanowire (AgNW) was spin-coated on polydimethylsiloxane (PDMS) substrate and subsequently dried. Then, PEDOT: PSS/PU nanocomposite was spin-coated over the AgNW/PDMS substrate and film was dried at 150°C for 1 hr. The PEDOT:PSS/PU nanocomposite was prepared by mixing PEDOT:PSS (5–8 wt% dimethyl sulfoxide (DMSO) & 1 wt% zonyl) with 4 wt% polyurethane dispersion (PU). The morphology of the fabricated film was measured through FE-SEM image and result was shown in **Figure 6a**. The resultant FE-SEM
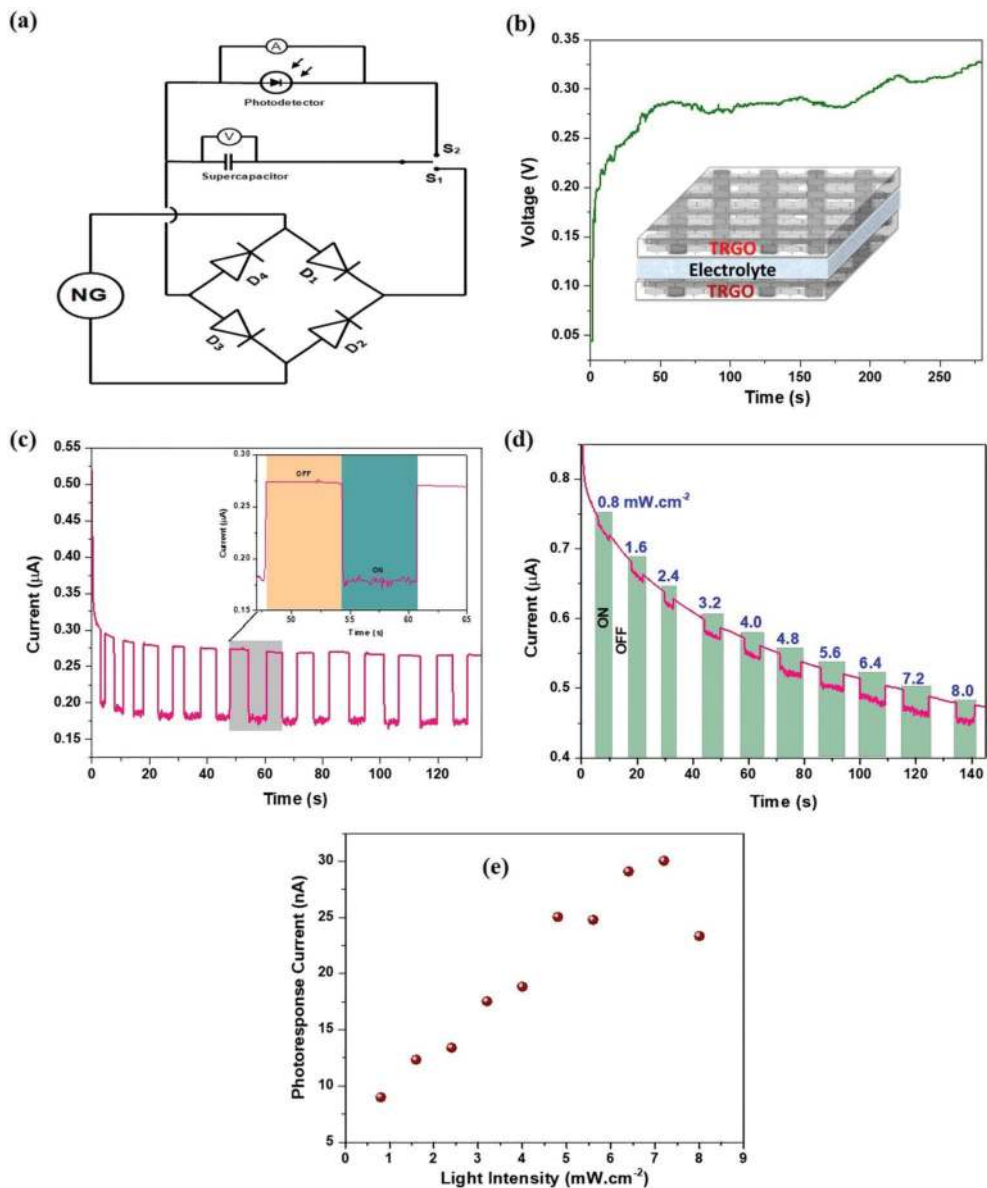
Figure 5. (a) Electric circuit diagram of the self-powered photosensor. (b) Charging of F-SCs by piezoelectric nanogenerator; inset is the structure of F-SC. (c) Time-dependent response of multiple ON/OFF cycles at a constant illumination intensity of 8 mW cm⁻² at λ = 365 nm. (d) Time-dependent photoresponse with different illumination intensity. (e) Photoresponse current versus light intensity. Figure is adapted with permission from the Ref. [19]. Copyright of Elsevier.

image is clearly indicating that the deposition of Ag NWs on the flexible PDMS substrate and Ag NWs are randomly oriented on the substrate. Further, spin-coating PEDOT:PSS/PU
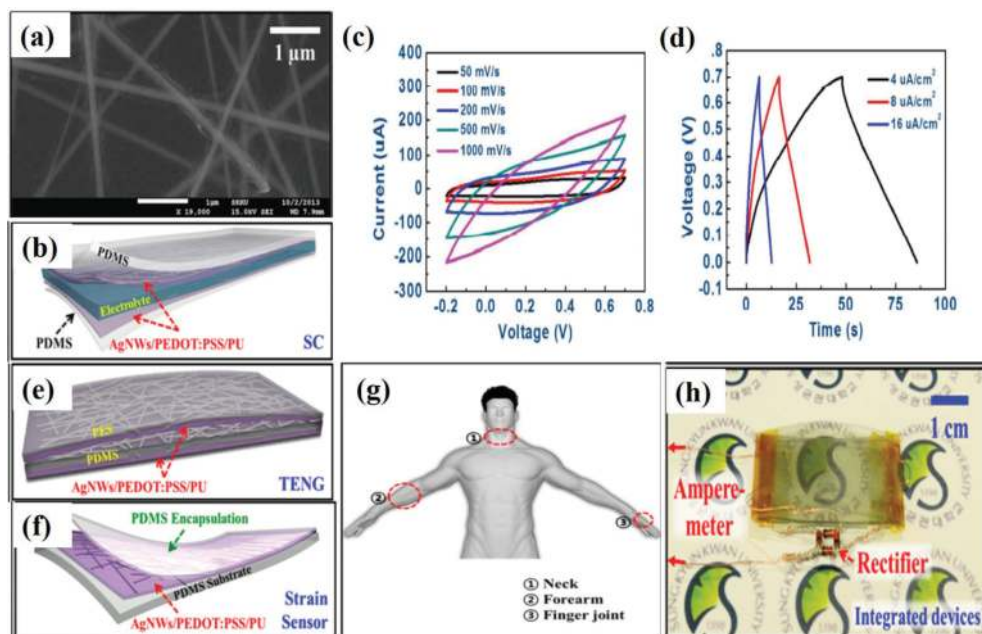
Figure 6. (a) FE-SEM image of the AgNW/PEDOT:PSS/PU film on PDMS substrate. (b) Schematic representation, (c) CV and (d) galvanostatic charge-discharge curves of the fabricated transparent flexible supercapacitor device. Schematic illustration of fabricated (e) TENG, (f) transparent strain sensor, and (g) strain sensor on different parts of human body. (h) Digital photograph of the self-powered strain sensor. Figure adapted with permission from the Ref. [23]. Copyright of American Chemical Society.

deposition eliminates the Ag NWs adhesive problems and connect silver nanowires. Moreover, deposition of PEDOT:PSS/PU nanocomposite provides higher flexibility and stretchability to the device by embedding the Ag NW inside polymer matrices. Finally, the flexible supercapacitor device was fabricated by sandwiching poly(vinyl alcohol)/phosphoric acid (PVA/H_3PO_4) film between two PDMS/AgNW/PEDOT: PSS/PU substrate [23]. The transparent, stretchable supercapacitor device was schematically illustrated in **Figure 6b**. The performance of the fabricated flexible supercapacitor device was evaluated based on CV and GCD curves at a different scan rate and current densities and results displayed in **Figure 6**c and d. The fabricated PDMS/AgNW/PEDOT:PSS/PU symmetric supercapacitor delivered a maximum areal capacitance of 190 μF cm^{-2} and 396 μF cm^{-2} at a scan rate of 50 mV s^{-1} and a current density of 4 μA cm^{-2}, respectively.

2.2.1. Fabrication and characterization of transparent, stretchable self-powered patchable sensor

The arch type triboelectric nanogenerator (TENG) device was fabricated by placing an arch-shaped PES/AgNW/PEDOT:PSS/PU on PDMS/AgNW/PEDOT:PSS/PU and schematic was shown in **Figure 6e**. The fabricated device designed to contact the arch-shaped PES surface with PDMS surface. The transparent, stretchable strain sensor was fabricated same as

supercapacitor electrode and additionally, PDMS layer was covered over the electrode to avoid the delamination and increase the stretchable nature. Here, AgNW/PEDOT:PSS/PU coated PDMS substrate was used as an active strain sensor and schematic representation of the fabricated electrode was given in **Figure 6f**. Further, the schematic representation of strain sensor placed on different parts of the human body is shown in **Figure 6g**. To demonstrate the capability of the fabricated strain sensor, it has integrated with supercapacitor device. The original
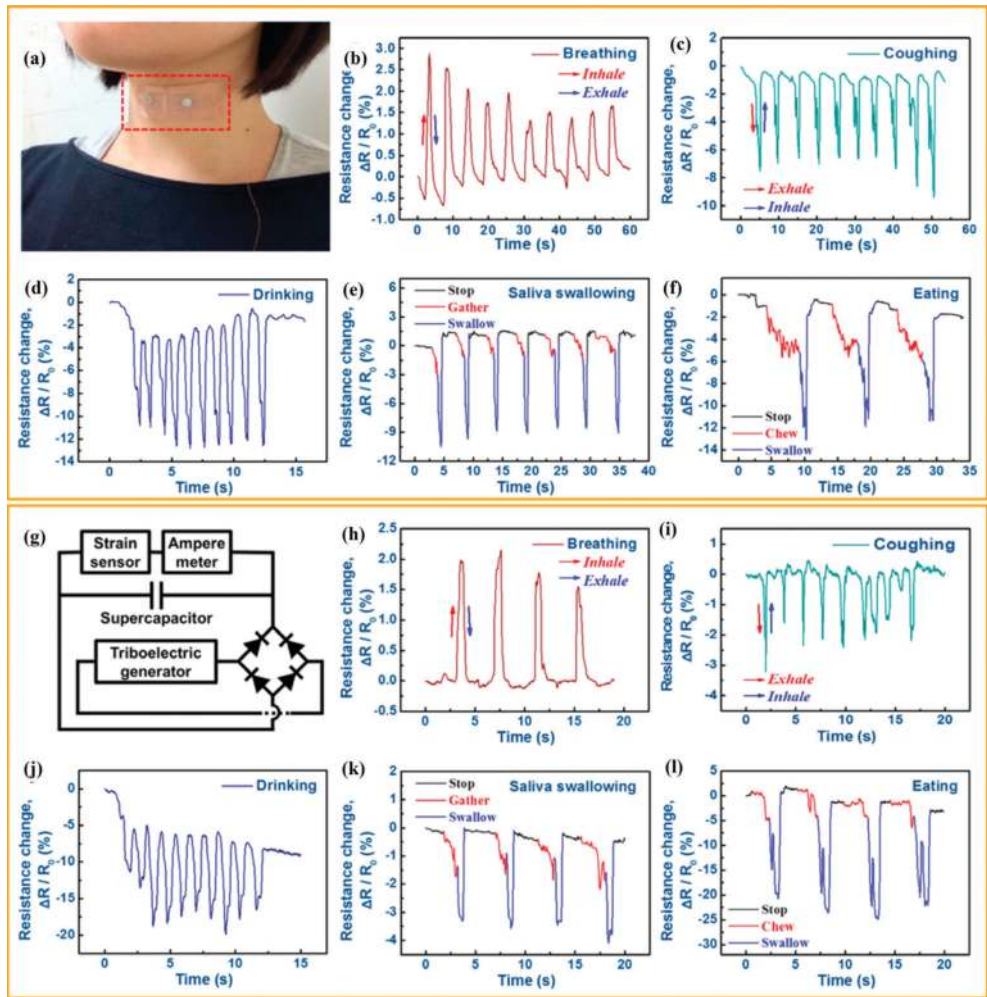

Figure 7. Monitoring of strain caused by muscle movement for functions of the trachea and esophagus. (a) Stretchable and transparent strain sensor attached to the neck. Resistance change ($\Delta R/R_0$) of the strain sensor versus time measured by source measurement unit, (b) breathing, (c) coughing, (d) drinking, (e) saliva swallowing, and (f) eating. (g) Circuit diagram of strain according to the sensor with SC charged by TENG. Resistance change ($\Delta R/R_0$) of the strain sensor versus time measured by SC charged by TENG, through (h) breathing, (i) coughing, (j) drinking, (k) saliva swallowing, and (l) eating, respectively. Figures are reproduced with permission from Ref. [23]. Copyright of American Chemical Society.

photocopy of the integrated device was shown in **Figure 6h**. The ability of the fabricated device was calibrated by attaching the device at neck to monitor the muscle movements of the trachea during breathing and coughing and esophagus during drinking, swallowing, and eating. At first, the integrated device was charged by the external power source and used to run the strain sensor. The measured output signal from the embedded device was shown in **Figure 7**, and it is clear that the fabricated device highly sensitive to the muscle movement, well distinguishable between the nature of applied strain. To demonstrate the self-powered operation of the integrated device, the supercapacitor was charge through the triboelectric nanogenerator by mechanical vibration (pushing). The charging performance of the supercapacitor device with integrated TENG was shown in **Figure 8**. The results indicating that the integrated supercapacitor device charge up to 0.9 V at the short period (1500 s) of mechanical vibration.

Further, the self-charged power was used to power the strain sensor to monitor the muscle movement. The output performance of the sensor powered by self-charged supercapacitor device is highly sensitive and almost same type of response observed as like externally charged device. The output performance of the strain sensor was given in **Figure 7h–i**. Similarly, the fabricated device showed higher sensitivity to the various human body activity like twisting, turning the wrist, clenching, etc. This result opens up to use self-powered systems for multiple application in wearable application as well internet of things (IoT).

2.3. Fabrication and integration of supercapacitor device with solar energy harvesters

2.3.1. Synthesis and characterization of 3D-NiCo$_2$O$_4$/Ni fiber electrodes

The three dimensional (3D) porous nickel (Ni) films on metal fiber substrate were deposited using electrodeposition with a hydrogen bubble template method [62]. Briefly, the 3D porous Ni film was electrodeposited at a constant current of 2.5 A using DC power supply with the electrolyte containing a 0.1 M NiCl$_2$ and 2 M NH$_4$Cl and then dried at 60°C for 12 h in hot air over. The 3D-NiCo$_2$O$_4$/Ni nanostructures were prepared by the electrodeposition of
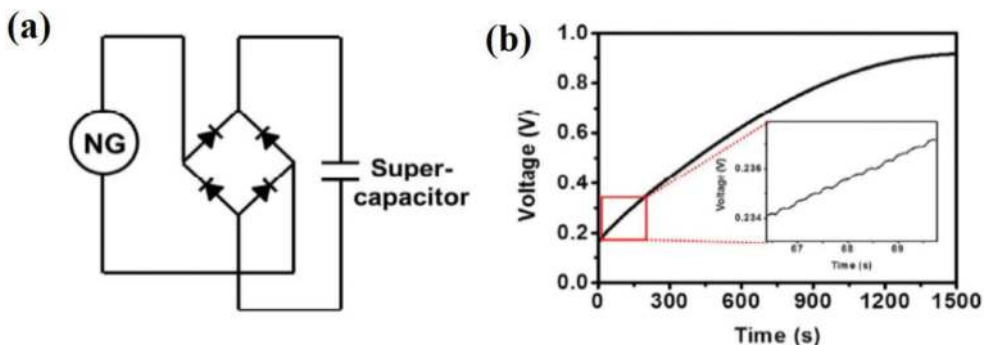

Figure 8. Charging property of the transparent and stretchable SC charged by a TENG. (a) Schematic of the rectifying circuit and SC. (b) Charging curve of the SC charged by the power generated by the TENG, and charging steps of the SC (inset). Figure is adapted with permission from the Ref. [23]. Copyright of American Chemical Society.

bimetallic (Ni, Co) hydroxide in a standard three-electrode system in an aqueous solution containing 1:2 molar ratio of 0.02 M nickel nitrate ($Ni(NO_3)_2.6H_2O$) and 0.04 M cobalt nitrate ($Co(NO_3)_2.6H_2O$) at a constant potential of -1 V for 5 min and followed by thermal transformation into spinel $NiCo_2O_4$ at 300°C for 2 h [63]. The construction of 3D architectures electrode would be predictable to exhibit better electrochemical performance in terms of high specific capacitance, high-rate capability, and high energy density. The expectation of enriched performance is mainly due to the enlarged active surface area and open pores which facilitates the diffusion of electrolyte, highly porous interconnected network of nickel metal improves the fast electron transport, the large surface area of electrode contact with the electrolyte as well as lower resistance, better adhesion between the substrate and electroactive material.

The morphology of 3D porous Ni films and 3D-$NiCo_2O_4$/Ni nanostructures were examined by FE-SEM. **Figure 9a–b**. depicts the 3D porous interconnected Ni dendritic walls. The dendritic walls were composed of numerous interlinked nanoparticles and display continuous interspaces. The FE-SEM images of 3D-$NiCo_2O_4$/Ni (**Figure 9c–d**) shows the highly porous flower-like nanostructures over the Ni surface. The elemental composition of the as-prepared 3D-$NiCo_2O_4$/Ni nanostructure film was evaluated by energy-dispersive X-ray spectroscopy and shown in **Figure 9e–f**. The Energy-dispersive X-ray spectroscopy (EDS) spectrum shows the distinctive peaks of Ni, Co and O elements present in the sample, which confirmed the formation of 3D-$NiCo_2O_4$/Ni. Further, the elemental mapping images clearly display the uniform distribution of Ni, Co and O elements within the 3D-$NiCo_2O_4$/Ni structure. Also, XRD spectrum of 3D-$NiCo_2O_4$/Ni exhibited the distinct diffraction peaks at the diffraction angles of 37.1°, 59.1° and 64.9° correspond to the (311), (511) and (440) plane reflections of spinel $NiCo_2O_4$ crystalline structure (JCPDS file no: 20-0781). The electrochemical characterization of as-prepared electrode was analyzed by CV and GCD curves in 2 M KOH electrolyte. **Figure 9g–h** shows the CV and GCD curves of 3D-$NiCo_2O_4$/Ni fiber electrodes. The CV curves of the 3D-$NiCo_2O_4$/Ni electrodes show two pairs of redox peaks during the electrochemical process, which attributed to the reversible faradaic redox processes of Ni^{2+}/Ni^{3+} and Co^{2+}/Co^{3+} transitions [64]. Further, the GCD curves also exhibited a non-linear behavior with voltage plateau indicated the faradaic behavior of the electrodes. The calculated volumetric and gravimetric capacitance of the 3D-$NiCo_2O_4$/Ni fiber electrodes were 29.7 F cm^{-3} and 300 F g^{-1}, respectively.

Flexible solid-state fiber supercapacitor based on two 3D-$NiCo_2O_4$/Ni used as a positive and negative electrode, with polyvinyl alcohol- potassium hydroxide (PVA-KOH) gel electrolyte on a polyethylene terephthalate (PET) substrate was fabricated, for real-world applications. The two electrodes were assembled in parallel with separation of 1 mm on the PET substrate using PVA-KOH. The typical CV curves of F-SC at different scan rates as shown in **Figure 10a**, signifying the typical pseudocapacitive behavior. **Figure 10b**. shows the GCD curves of F-SC at different current densities. The GCD curves of F-SC also reveal symmetry and linear in nature, confirms that the device has excellent electrochemical reversibility and capacitive behavior. The calculated gravimetric and volumetric capacitance of the full cell is 18.8 F g^{-1} and 1.86 F cm^{-3}, respectively. Further, the F-SC exhibited excellent cyclic stability (**Figure 10c**), even after 5000 cycles, with a capacitance retention of ~ 100%. The key parameter of the F-SC such as energy density and power density was calculated from the GCD curves (**Figure 10d**).

Figure 9. FE-SEM images of 3D-Ni (a-b) and 3D-NiCo$_2$O$_4$/Ni (c-d) nanostructures. (e) EDS and (f) X-ray diffraction (XRD) spectra of 3D-NiCo$_2$O$_4$/Ni. (g) CV and (h) GCD curves of 3D-NiCo$_2$O$_4$/Ni. Figure is adapted with permission from the Ref. [7]. Copyright of Royal Society of Chemistry.
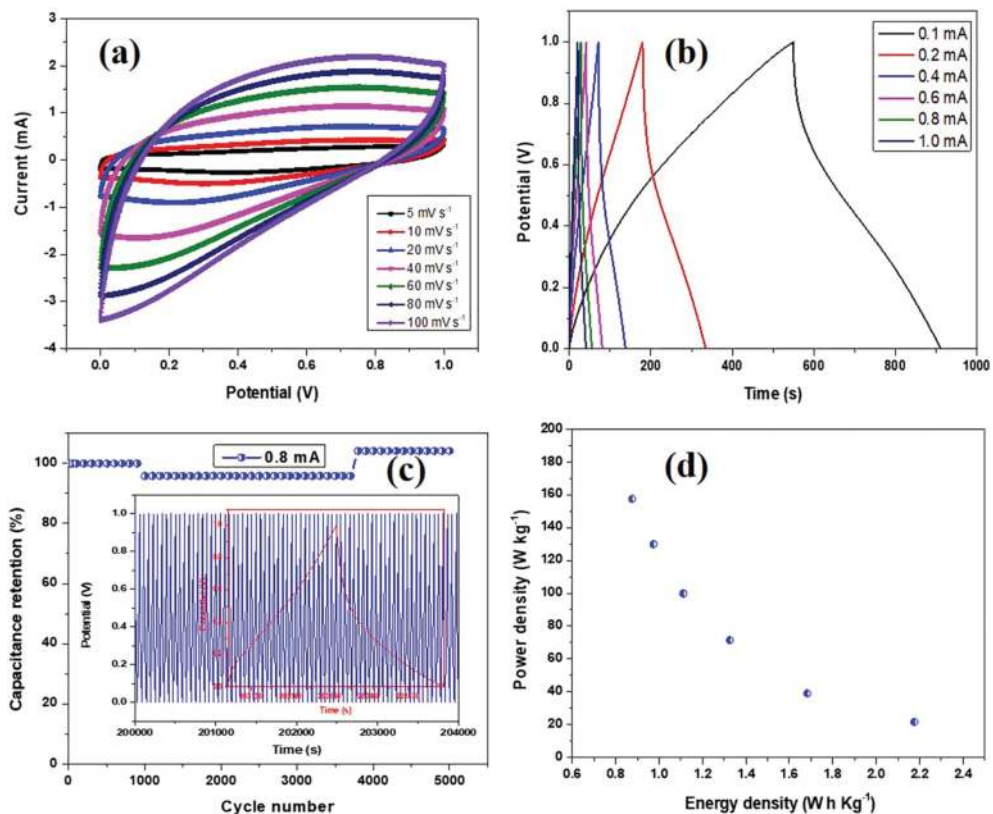
Figure 10. (a) Cyclic voltammograms of F-SC at different scan rates. (b) Galvanostatic charge/discharge profiles of F-SC at various currents. (c) the charge/discharge stability of F-SC at 0.8 mA. (d) Ragone plot of the F-SC. Reproduced from Ref. [7] with permission from the Royal Society of Chemistry.

The calculated energy density and power density of the F-SC is 2.18 W h kg^{-1} (0.21 mWh cm^{-3}) and 21.6 W kg^{-1} (2.1 mW cm^{-3}). The obtained values are higher than or comparable to previously reported F-SCs [20, 65–67].

2.3.2. Fabrication and characterization of dye-sensitized solar cells (DSSCs)

The fabrication and photovoltaic characterization of the DSSC as follows. First, TiCl$_4$ treatment was conducted by immersing the cleaned FTO glass in the 40 mM titanium tetrachloride (TiCl$_4$) solution for 30 min at 70°C. Then, the photoanode TiO$_2$ paste was deposited on the TiCl$_4$ treated FTO glass by doctor blade process followed by calcination at 550°C for 1 h. After that, the dye coating was performed by dipping the as-prepared TiO$_2$ in 0.5 mM of N-719 in tert-butanol/acetonitrile solution (1:1 vol.) for 12 h. The Pt counter electrode (CE) was deposited on the drilled FTO glass by spin-coating (2000 rpm, 2 times) using 30 mM of the H$_2$PtCl$_6$

solution in isopropyl alcohol (IPA) and annealed at 450 °C for 30 min. The working electrode and CE were assembled using 60 μm of Surlyn, and an electrolyte (0.5 M 1-hexyl-2,3-dimethylimidazolium iodide (C-tri), 0.02 M iodine, 0.5 M 4-tert-butylpyridine, and 0.05 M lithium iodide in acetonitrile) was added through a pre-drilled hole.

2.3.3. Integration and functional characterization of self-powered device

To demonstrate self-powered application, the fabricated fiber supercapacitor was integrated with DSSC and LED. The schematic illustration of the self-powered device is shown in **Figure 11a**. The self-powered system comprises of four series-connected DSSCs and three series F-SC and light emitting diode (LED). Here, DSSC served as an energy source to harvest the energy from sunlight and then to charge the supercapacitor. After that stored energy was utilized to drive LED without disruption. Initially, the F-SCs was charged with turning the switch S1 is on to connect DSSCs to the circuit. **Figure 11b** shows the current density-voltage curve of the serially-wound DSSCs. The open-circuit voltage, short-circuit current, and power conversion efficiency of the serially-wound DSSCs was 3.08 V, 3.94 mA cm^{-2}, and 6.96%, respectively. The inset of **Figure 11b** shows the digital photograph of serially-wound DSSCs. The F-SC charged from 0 to 3.2 V about 60s signifying the stable output of DSSCs as shown in **Figure 11c**. Afterwards, to demonstrate the self-powered operation, by turning the switch S2 is on, while switch S1 is off to illuminate the commercial green LED (**Figure 11c**) using charged supercapacitors. This study validated that fiber supercapacitors could store solar energy harvested from DSSCs, which suggests their massive application potential in diverse electronic devices.

2.4. Fabrication and integration of supercapacitor device with hybrid (solar and vibrational) energy harvesters

In this work, hybridized self-charging power textile system was developed by Wen et al., [68] to simultaneously collect outdoor/indoor sunlight and casual body movement energies and stored in an energy storage device for sustainable operation of wearable electronics. **Figure 12** shows the schematic illustration of hybridized self-charging power textile. The self-charging power textile system consists of fiber-shaped dye-sensitized solar cells (F-DSSC, top layer),
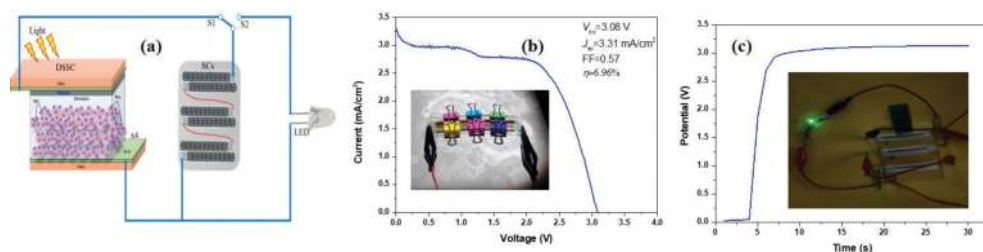

Figure 11. (a) Schematic diagram of the integration of F-SCs with DSSCs and LED. (b) J-V curve of the DSSCs connected in series under 1 sun irradiation. Inset is the digital image of four DSSCs assembled in series. (c) Charging curve of F-SCs module by DSSCs module in series; the inset is the digital photograph of green LED driven by F-SCs charged using DSSCs. Figure is adapted with permission from the Ref. [7]. Copyright of Royal Society of Chemistry.
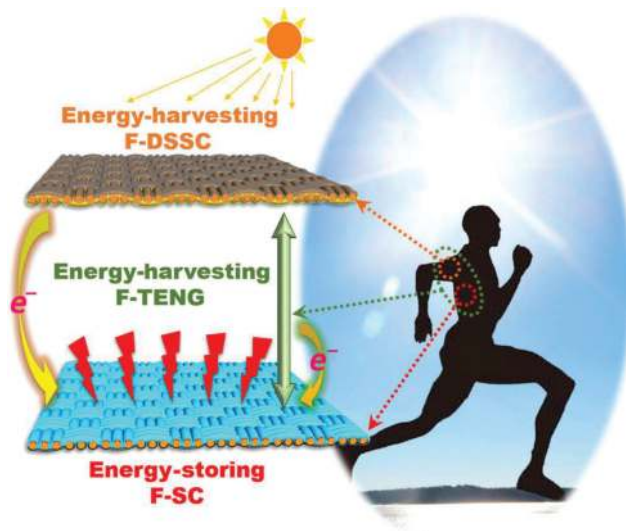
Figure 12. Schematic representation of the self-charging power textile. Reproduced from Ref. [68] with permission from the American Association for the Advancement of Science.

fiber-shaped triboelectric nanogenerator (F-TENG, middle layer) and fiber-shaped supercapacitors (F-SC, bottom layer). In this architecture, each solar cell and supercapacitor unit is coupled to one another, making a single triboelectric nanogenerator unit is assembled to scavenge body motion energy simultaneously. Both of the harvested energies could be effortlessly converted into electricity by using several solar cell units (for solar energy) and TENG (for random body motion energy) and then stored as chemical energy in supercapacitor modules for the operation of wearable electronics.

2.4.1. Fabrication and characterization of fiber-shaped supercapacitors

The binder-free $RuO_2 \cdot xH_2O$ on carbon fiber electrode was synthesized using a vapor-phase hydrothermal technique [69]. Briefly, a Ruthenium(III) chloride ($RuCl_3$) slurry prepared from 0.1 g of $RuCl_3$ and 4 ml of EtOH was coated onto the carbon fibers and dried at 60°C. Then the $RuCl_3$ coated carbon fibers were placed in a 50-ml Teflon-lined stainless steel autoclave with 0.1 M NaOH solution in an oven at 190°C for 5 h to get $RuO_2 \bullet xH_2O$-coated carbon fibers. Then, two fiber electrodes were closely assembled into the PDMS-covered Cu-coated tube and separated by a paper septum to form an all-solid-state flexible fiber-shaped supercapacitor. Before assembling, the fiber electrodes were immersed in a PVA/H_3PO_4 gel electrolyte for 10 min. **Figure 13a** shows the schematic representation of $RuO_2 \cdot xH_2O$ F-SC. The structural and morphological properties of the as-prepared electrodes were confirmed through SEM and XRD analysis. The SEM image (**Figure 13b–d**) of as-prepared fiber electrode shows the cracked mud morphology and the diameter of the fiber are ~10 mm. The XRD pattern of $RuO_2 \bullet xH_2O$ coated carbon fiber electrodes revealed an amorphous with partly rutile crystalline structure [70]. The electrochemical performance of F-SC was evaluated by CV and GCD techniques. **Figure 13e**

shows the CV curves of F-SC at different scan rates. It can be observed that the CV curves are maintained their initial shape even at higher scan rates, revealed their good capacitive behavior and better rate capability. The GCD curves of F-SC at various current densities were shown in **Figure 13f**. The GCD curves displayed the symmetric and triangle in shape under various current densities, confirmed the good capacitive behavior. The calculated energy specific capacitance and energy density of F-SC is 1.9 mF cm^{-1} and 1.37 mJ cm^{-1}, respectively. Further, the F-SC better cycling stability even after 5000 cycles with no obvious capacitance change as well as excellent mechanical stability under various bending conditions (from 0° to 180°).

2.4.2. Fabrication and functional characterization of fiber-shaped hybrid energy harvester using dye-sensitized solar cells and triboelectric nanogenerator

Firstly, a photoanode (TiO$_2$ nanotube) was prepared on Ti wire surface by anodization techniques in a solution containing 0.3 wt % NH$_4$F/EG and 8 wt % H$_2$O at 60 V for 6 h using a two-electrode cell with Pt wire as a counter electrode [71]. After that, the anodized Ti wire was annealed at 500°C for 1 h and then immersed in 40 mM TiCl$_4$ solution at 70°C for 30 min. Afterwards, the as-prepared samples were annealed again at 450°C for 30 min. Secondly, the
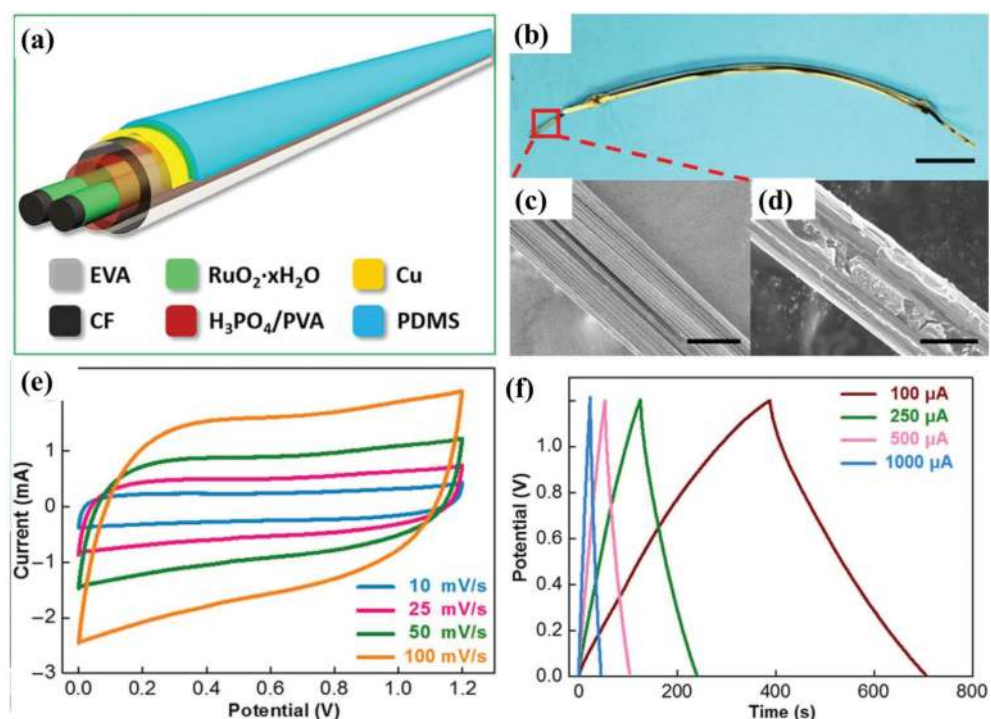

Figure 13. (a) Schematic diagram and (b) photograph of F-SC. (c-d) SEM images of RuO$_2$·xH$_2$O-coated carbon fiber electrode. (e) CV and (f) GCD curves of F-SC at various scan rates and current densities. Figure is adapted with permission from the Ref. [68]. Copyright of American Association for the Advancement of Science.

prepared photoanode was immersed in a 3×10^{-4} M of N719 dye solution in ACN and tBA (v/v = 1/1) at room temperature for 24 h. Thirdly, the platinum counter electrode was fabricated by soaking carbon fiber in an $H_2PtCl_6 \bullet 6H_2O$ aqueous solution (5 mg/ml) for 5 min followed by thermal treatment at 400°C for 30 min. Finally, F-DSSC was fabricated by inserting a Pt-coated carbon fiber and a dye-sensitized Ti photo anode into the Cu-coated ethylene vinyl acetate (EVA) tube in parallel and then injected an electrolyte into the tubing (0.1 M LiI, 0.05 M I2, 0.6 M DMPII, and 0.5 M tBP in MPN). Finally, the pipe was sealed with sealing glue to prevent the electrolyte leakage. The schematic illustration and digital photograph of F-DSSC are shown in **Figure 14a**. Vertically oriented arrays of TiO_2 nanotubes with a diameter of ~50 nm on Ti wires surface were confirmed through SEM images (**Figure 14b–d**). The current density-voltage (J-V) characteristic of F-DSSC was assessed under standard illumination (100 mW cm − 2; AM1.5). The short-circuit current density, open-circuit voltage, fill factor, and power conversion efficiency of the F-DSSC is 11.92 mA cm^{-2}, 0.74 V, 0.64, and 5.64%, respectively.

A fiber-shaped triboelectric nanogenerator (F-TENG) was fabricated by connecting a Cu-coated EVA tube as a triboelectric electrode and the PDMS-covered Cu-coated EVA tube as another electrode. The copper (Cu) electrode with 1 mm thickness was deposited onto the EVA tubing surface by physical vapor deposition at 100 W in Ar atmosphere for 40 min. Then, the PDMS-covered Cu-coated EVA tubing was deposited by dip-coating process [72, 73] and dried at room temperature for 12 h. **Figure 14e–f** displays the schematic diagram and a digital photograph of F-TENG. The output performance of the fabricated F-TENG was studied through the periodic contact and separation under different frequencies. The open-circuit voltage (~12.6 V) and charge of the device are almost constant (~4.5 nC,) when the frequencies vary from 1 to 5 Hz, but the short-circuit current (ISC) increased from ~0.06 to ~0.15 μA. These result confirmed that the fabricated device could harvest the renewable energy efficiently.

2.4.3. Fabrication and testing of the hybridized self-charging power textile

The hybridized self-charging power textile was fabricated by intertwined several solar cells and supercapacitors into the fabric to form a textile structure with serial/parallel connection (tune the output voltage and capacitance of devices to drive real wearable electronics). The textile-based F-TENG system was constructed by assembling the intertwined F-DSSC textile
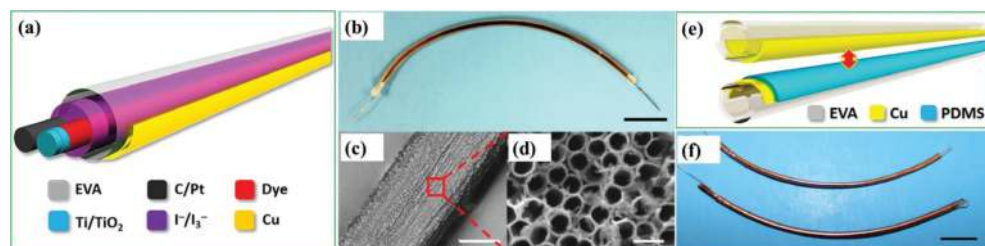

Figure 14. (a) Schematic diagram and (b) photograph of F-DSSC. (c-d) SEM images of TiO_2 nanotube arrays. (e) Schematic illustration and (f) digital photograph of F-TENG. Figure is adapted with permission from the Ref. [68]. Copyright of American Association for the Advancement of Science.

fabric as the top layer to harvest solar energy, and the bottom layer of intertwined F-SC textile was used to store harvested energies. Meanwhile, both woven textiles instantaneously engage in recreation as triboelectric layers to collect mechanical energies from human body motion, which were also stored in F-SC after rectification.

To check the real-time applications, the fabricated textile device was attached with a T-Shirt (**Figure 15**) and harvests both sunlight as well as body motion in outdoor and indoor activities, respectively. The whole device consists of three F-DSSC and 6 F-SC units in serial and then intertwined separately in a 3 × 3 network. The demonstration of self-charging power textile under outdoor and indoor activities is shown in **Figure 15a–c**. **Figure 15d** shows the equivalent circuit of hybridized self-charging power textile. Herein, an AC generated from F-TENG was converted into DC by a bridge rectifier, and it stored in F-SC. Moreover, a diode in the circuit blocks the inflow current through an F-DSSC. The self-charging characteristic was achieved by harvesting solar and mechanical energies from human motion through the as-fabricated hybrid device and is presented in **Figure 15e**. Initially, the F-SC was charged through a turn on the switch S0 and S1, which connect F-DSSC to F-SC, while the S2 switch is in off. The stable F-DSSCs output charge the F-SC to 1.8 V from 0 at 69 s. The F-SCs charging voltage persists at 1.8 V, due to the low output voltage of the F-DSSCs, which limits their reliability and practicability and it indicated by light blue-shaded area in **Figure 15e**. Further, the F-SCs can be charged continuously to a higher voltage as highlighted (light red-shaded area)
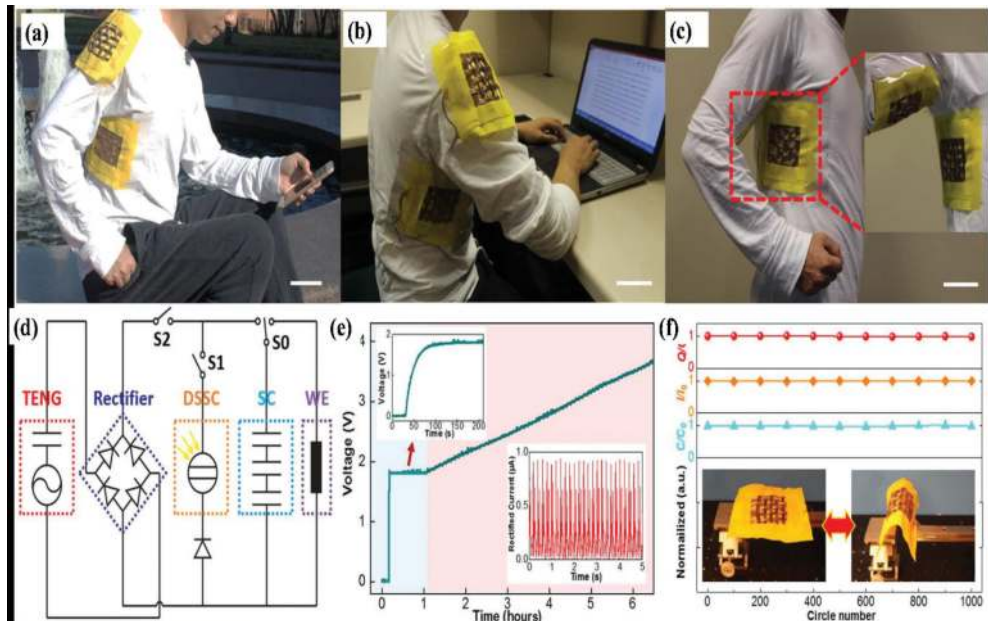

Figure 15. Demonstration of the self-charging powered textile. Digital photograph of the hybrid device under outdoor (a), indoor (b), and movement (c) environments. (d) the equivalent circuit of the self-charging powered textile for portable electronics. (e) the self-charging curve of the F-DSSC and F-TENG hybrid. (f) Durability studies of the fabricated devices for 1000 cycles. Insets show the photographs of bending status between 0° and 180°. Reproduced from Ref. [68] with permission from the American Association for the Advancement of Science.

in charging curves through F-TENGs by turn on the S2 switch. Then the charged F-SCs can power the portable electronic devices including LEDs, smart watches, sensors, etc. Moreover, the charging efficiency can be improved through impedance matching of DSSCs, TENGs, and SCs. Finally, the stability of the fabricated device was tested under continuous bending motion for 1000 cycles using the linear motor, as shown in **Figure 15f**. The advancement in the present efforts provides a new path for self-powered systems in wearable technology.

3. Conclusion

In summary, a self-powered system was successfully demonstrated by charging the supercapacitor using an energy harvester and powered a photosensor as well as portable devices. The various results showed the feasibility of using a supercapacitor as an efficient energy storage components and their application in self-powered devices due its high power density (uptake pulses) leads to the high energy conversion and storage efficiency. This work offers a welcome advancement in the supercapacitor toward the self-powered system application in flexible/wearable technology, which will pledge promising developments in self-powered flexible displays, infrastructure, and environmental monitoring, internet of things, defense technologies and wearable electronics (artificial electronic skin, smart textiles/watch straps), among others.

Acknowledgements

Author details

Ananthakumar Ramadoss[1,2], Balasubramaniam Saravanakumar[1,3,4] and Sang-Jae Kim[1]*

*Address all correspondence to: kimsangj@jejunu.ac.kr

1 Nanomaterials and System Lab, Department of Mechatronics Engineering, Jeju National University, Jeju, Republic of Korea

2 Laboratory for Advanced Research in Polymeric Materials, Central Institute of Plastic Engineering and Technology, Bhubaneswar, India

3 School of Chemistry and Environment, South China Normal University, Guangzhou, China

4 Engineering Research Center of MTEES (Ministry of Education), Research Center of BMET (Guangdong Province), Engineering Laboratory of OFMHEB (Guangdong Province), Key Laboratory of ETESPG (GHEI) and Innovative Platform for ITBMD (Guangzhou Municipality), South China Normal University, Guangzhou, China

References

[1] Nykvist B, Nilsson M. Rapidly falling costs of battery packs for electric vehicles. Nature Climate Change. 2015;**5**:329-332

[2] Yu G, Gao J, Hummelen JC, Wudl F, Heeger AJ. Polymer photovoltaic cells: Enhanced efficiencies via a network of internal donor-acceptor heterojunctions. Science. 1995;**270**:1789

[3] Ma W, Yang C, Gong X, Lee K, Heeger AJ. Thermally stable, efficient polymer solar cells with nanoscale control of the interpenetrating network morphology. Advanced Functional Materials. 2005;**15**:1617-1622

[4] Kim J, Lee SM, Hwang YH, Lee S, Park B, Jang JH, et al. A highly efficient self-power pack system integrating supercapacitors and photovoltaics with an area-saving monolithic architecture. Journal of Materials Chemistry A. 2017;**5**:1906-1912

[5] Chu S, Majumdar A. Opportunities and challenges for a sustainable energy future. Nature. 2012;**488**:294-303

[6] Ramadoss A, Yoon KY, Kwak MJ, Kim SI, Ryu ST, Jang JH. Fully flexible, lightweight, high performance all-solid-state supercapacitor based on 3-dimensional-graphene/graphite-paper. Journal of Power Sources. 2017;**337**:159-165

[7] Ramadoss A, Kang KN, Ahn HJ, Kim SI, Ryu ST, Jang JH. Realization of high performance flexible wire supercapacitors based on 3-dimensional $NiCo_2O_4$/Ni fibers. Journal of Materials Chemistry A. 2016;**4**:4718-4727

[8] Xu X, Li S, Zhang H, Shen Y, Zakeeruddin SM, Graetzel M. A power pack based on organometallic perovskite solar cell and supercapacitor. ACS Nano. 2015;**9**:1782-1787

[9] Saito Y, Ogawa A, Uchida S, Kubo T, Segawa H. Energy-storable dye-sensitized solar cells with interdigitated nafion/polypyrrole-Pt comb-like electrodes. Chemistry Letters. 2010;**39**:488-489

[10] Simon P, Gogotsi Y. Materials for electrochemical capacitors. Nature Materials. 2008;**7**:845-854

[11] Wang J, Li X, Zi Y, Wang S, Li Z, Zheng L, et al. A flexible fiber-based supercapacitor-triboelectric-nanogenerator power system for wearable electronics. Advanced Materials. 2015;**27**:4830-4836

[12] Wang ZL, Song J. Piezoelectric nanogenerators based on zinc oxide nanowire arrays. Science. 2016;**312**:242

[13] Gao PX, Song J, Liu J, Wang ZL. Nanowire piezoelectric nanogenerators on plastic substrates as flexible power sources for Nanodevices. Advanced Materials. 2007;**19**:67-72

[14] Miller JR, Simon P. Electrochemical capacitors for energy management. Science. 2008;**321**:651

[15] Kötz R, Carlen M. Principles and applications of electrochemical capacitors. Electrochimica Acta. 2000;**45**:2483-2498

[16] Wang G, Zhang L, Zhang JA. Review of electrode materials for electrochemical superca-pacitors. Chemical Society Reviews. 2012;**41**:797-828

[17] Guo W, Xue X, Wang S, Lin C, Wang ZL. An integrated power pack of dye-sensitized solar cell and li battery based on double-sided TiO_2 nanotube arrays. Nano Letters. 2012;**12**: 2520-2523

[18] Wang X, Liu B, Liu R, Wang Q, Hou H, Chen D, et al. Fiber-based flexible all-solid-state asymmetric supercapacitors for integrated photodetecting system. Angewandte Chemie, International Edition. 2014;**53**:1849-1853

[19] Ramadoss A, Saravanakumar B, Kim SJ. Thermally reduced graphene oxide-coated fab-rics for flexible supercapacitors and self-powered systems. Nano Energy. 2015;**15**:587-597

[20] Xiao X, Li T, Yang P, Gao Y, Jin H, Ni W, et al. Fiber-based all-solid-state flexible super-capacitors for self-powered systems. ACS Nano. 2012;**6**:9200-9206

[21] Yang P, Xiao X, Li Y, Ding Y, Qiang P, Tan X, et al. Hydrogenated ZnO core-shell nanoca-bles for flexible supercapacitors and self-powered systems. ACS Nano. 2013;**7**:2617-2626

[22] Jung S, Lee J, Hyeon T, Lee M, Kim DH. Fabric-based integrated energy devices for wearable activity monitors. Advanced Materials. 2014;**26**:6329-6334

[23] Hwang BU, Lee JH, Trung TQ, Roh E, Kim DI, Kim SW, et al. Transparent stretchable self-powered patchable sensor platform with ultrasensitive recognition of human activi-ties. ACS Nano. 2015;**9**:8801-8810

[24] Li D, Kaner RB. Graphene-based materials. Science. 2008;**320**:1170

[25] Stankovich S, Dikin DA, Dommett GHB, Kohlhaas KM, Zimney EJ, Stach EA, et al. Graphene-based composite materials. Nature. 2006;**442**:282-286

[26] Sun D, Yan X, Lang J, Xue Q. High performance supercapacitor electrode based on gra-phene paper via flame-induced reduction of graphene oxide paper. Journal of Power Sources. 2013;**222**:52-58

[27] Tan YB, Lee JM. Graphene for supercapacitor applications. Journal of Materials Chemistry A. 2013;**1**:14814-14843

[28] Xu C, Xu B, Gu Y, Xiong Z, Sun J, Zhao XS. Graphene-based electrodes for electrochemi-cal energy storage. Energy & Environmental Science. 2013;**6**:1388-1414

[29] Kim KS, Zhao Y, Jang H, Lee SY, Kim JM, Kim KS, et al. Large-scale pattern growth of graphene films for stretchable transparent electrodes. Nature. 2009;**457**:706-710

[30] Xuekun L, Minfeng Y, Hui H, Rodney SR. Tailoring graphite with the goal of achieving single sheets. Nanotechnology. 1999;**10**:269

[31] Berger C, Song Z, Li X, Wu X, Brown N, Naud C, et al. Electronic confinement and coherence in patterned epitaxial graphene. Science. 2006;**312**:1191

[32] Choucair M, Thordarson P, Stride JA. Gram-scale production of graphene based on solvothermal synthesis and sonication. Nature Nanotechnology. 2009;**4**:30-33

[33] Stankovich S, Dikin DA, Piner RD, Kohlhaas KA, Kleinhammes A, Jia Y. Synthesis of graphene-based nanosheets via chemical reduction of exfoliated graphite oxide. Carbon. 2007;**45**:1558-1565

[34] Park S, Ruoff RS. Chemical methods for the production of graphenes. Nature Nanotechnology. 2009;**4**:217-224

[35] Saravanakumar B, Mohan R, Kim SJ. Facile synthesis of graphene/ZnO nanocomposites by low temperature hydrothermal method. Materials Research Bulletin. 2013;**48**:878-883

[36] Zhang D, Zhang X, Chen Y, Wang C, Ma Y. An environment-friendly route to synthesize reduced graphene oxide as a supercapacitor electrode material. Electrochimica Acta. 2012;**69**:364-370

[37] Tuinstra F, Koenig JL. Raman spectrum of graphite. The Journal of Chemical Physics. 1970;**53**:1126-1130

[38] Chen C, Long M, Xia M, Zhang C, Cai W. Reduction of graphene oxide by an in-situ photoelectrochemical method in a dye-sensitized solar cell assembly. Nanoscale Research Letters. 2012;**7**:101

[39] Eda G, Chhowalla M. Chemically derived graphene oxide: Towards large-area thin-film electronics and optoelectronics. Advanced Materials. 2010;**22**:2392-2415

[40] Chen Y, Zhang X, Zhang D, Yu P, Ma Y. High performance supercapacitors based on reduced graphene oxide in aqueous and ionic liquid electrolytes. Carbon. 2011;**49**:573-580

[41] Xu B, Yue S, Sui Z, Zhang X, Hou S, Cao G, et al. What is the choice for supercapacitors: Graphene or graphene oxide? Energy & Environmental Science. 2011;**4**:2826-2830

[42] Lin Z, Liu Y, Yao Y, Hildreth OJ, Li Z, Moon K, et al. Superior capacitance of functionalized graphene. The Journal of Physical Chemistry C. 2011;**115**:7120-7125

[43] Ramadoss A, Kim SJ. Improved activity of a graphene–TiO_2 hybrid electrode in an electrochemical supercapacitor. Carbon. 2013;**63**:434-445

[44] Kaempgen M, Chan CK, Ma J, Cui Y, Gruner G. Printable thin film supercapacitors using single-walled carbon nanotubes. Nano Letters. 2009;**9**:1872-1876

[45] Li Y, van Zijll M, Chiang S, Pan N. KOH modified graphene nanosheets for supercapacitor electrodes. Journal of Power Sources. 2011;**196**:6003-6006

[46] Liu C, Yu Z, Neff D, Zhamu A, Jang BZ. Graphene-based supercapacitor with an ultra-high energy density. Nano Letters. 2010;**10**:4863-4868

[47] Zhu Y, Murali S, Stoller MD, Velamakanni A, Piner RD, Ruoff RS. Microwave assisted exfoliation and reduction of graphite oxide for ultracapacitors. Carbon. 2010;**48**:2118-2122

[48] Ramadoss A, Kim GS, Kim SJ. Fabrication of reduced graphene oxide/TiO_2 nanorod/ reduced graphene oxide hybrid nanostructures as electrode materials for supercapacitor applications. CrystEngComm. 2013;**15**:10222-10229

[49] Lee M, Balasingam SK, Jeong HY, Hong WG, Lee HBR, Kim BH, et al. One-step hydro-thermal synthesis of graphene decorated V_2O_5 nanobelts for enhanced electrochemical energy storage. Scientific Reports. 2015;**5**:8151

[50] Xu Y, Lin Z, Huang X, Liu Y, Huang Y, Duan X. Flexible solid-state supercapacitors based on three-dimensional graphene hydrogel films. ACS Nano. 2013;**7**:4042-4049

[51] Yu A, Roes I, Davies A, Chen Z. Ultrathin, transparent, and flexible graphene films for supercapacitor application. Applied Physics Letters. 2010;**96**:253105

[52] Choi BG, Chang SJ, Kang HW, Park CP, Kim HJ, Hong WH, et al. High performance of a solid-state flexible asymmetric supercapacitor based on graphene films. Nanoscale. 2012;**4**:4983-4988

[53] El-Kady MF, Strong V, Dubin S, Kaner RB. Laser scribing of high-performance and flex-ible graphene-based electrochemical capacitors. Science. 2012;**335**:1326

[54] Weng Z, Su Y, Wang DW, Li F, Du J, Cheng HM. Graphene-cellulose paper flexible super-capacitors. Advanced Energy Materials. 2011;**1**:917-922

[55] Choi BG, Hong J, Hong WH, Hammond PT, Park H. Facilitated ion transport in all-solid-state flexible supercapacitors. ACS Nano. 2011;**5**:7205-7213

[56] Kang YJ, Chun SJ, Lee SS, Kim BY, Kim JH, Chung H, et al. All-solid-state flexible super-capacitors fabricated with bacterial Nanocellulose papers, carbon nanotubes, and tri-block-copolymer ion gels. ACS Nano. 2012;**6**:6400-6406

[57] Meng C, Liu C, Chen L, Hu C, Fan S. Highly flexible and all-solid-state paperlike poly-mer supercapacitors. Nano Letters. 2010;**10**:4025-4031

[58] Yu Jin K, Haegeun C, Chi-Hwan H, Woong K. All-solid-state flexible supercapacitors based on papers coated with carbon nanotubes and ionic-liquid-based gel electrolytes. Nanotechnology. 2012;**23**:065401

[59] Hu S, Rajamani R, Yu X. Flexible solid-state paper based carbon nanotube supercapaci-tor. Applied Physics Letters. 2012;**100**:104103

[60] Meng C, Liu C, Fan S. Flexible carbon nanotube/polyaniline paper-like films and their enhanced electrochemical properties. Electrochemistry Communications. 2009;**11**:186-189

[61] Yang Q, Guo X, Wang W, Zhang Y, Xu S, Lien DH, et al. Enhancing sensitivity of a single ZnO micro-/nanowire photodetector by piezo-phototronic effect. ACS Nano. 2010;**4**: 6285-6291

[62] Xia XH, Tu JP, Zhang YQ, Mai YJ, Wang XL, Gu CD, et al. Three-dimentional porous Nano-Ni/co(OH)$_2$ Nanoflake composite film: A pseudocapacitive material with superior performance. The Journal of Physical Chemistry C. 2011;**115**:22662-22668

[63] Yuan C, Li J, Hou L, Zhang X, Shen L, Lou XW. Ultrathin mesoporous NiCo$_2$O$_4$ nanosheets supported on Ni foam as advanced electrodes for supercapacitors. Advanced Functional Materials. 2012;**22**:4592-4597

[64] Gupta V, Gupta S, Miura N. Electrochemically synthesized nanocrystalline spinel thin film for high performance supercapacitor. Journal of Power Sources. 2010;**195**:3757-3760

[65] Wang Q, Wang X, Xu J, Ouyang X, Hou X, Chen D, et al. Flexible coaxial-type fiber supercapacitor based on NiCo$_2$O$_4$ nanosheets electrodes. Nano Energy. 2014;**8**:44-51

[66] Gu S, Lou Z, Ma X, Shen G. CuCo$_2$O$_4$ nanowires grown on a Ni wire for high-performance, flexible fiber supercapacitors. ChemElectroChem. 2015;**2**:1042-1047

[67] Wu H, Lou Z, Yang H, Shen G. A flexible spiral-type supercapacitor based on ZnCo$_2$O$_4$ nanorod electrodes. Nanoscale. 2015;**7**:1921-1926

[68] Wen Z, Yeh MH, Guo H, Wang J, Zi Y, Xu W, et al. Self-powered textile for wearable electronics by hybridizing fiber-shaped nanogenerators, solar cells, and supercapacitors. Science Advances. 2016;**2**

[69] Park J, Lee JW, Ye BU, Chun SH, Joo SH, Park H, et al. Structural evolution of chemically-driven RuO$_2$ nanowires and 3-dimensional design for photo-catalytic applications. Scientific Reports. 2015;**5**:11933

[70] Wu ZS, Wang DW, Ren W, Zhao J, Zhou G, Li F, et al. Anchoring hydrous RuO$_2$ on graphene sheets for high-performance electrochemical capacitors. Advanced Functional Materials. 2010;**20**:3595-3602

[71] Yang Z, Deng J, Sun X, Li H, Peng H. Stretchable, wearable dye-sensitized solar cells. Advanced Materials. 2014;**26**:2643-2647

[72] Zhong J, Zhang Y, Zhong Q, Hu Q, Hu B, Wang ZL, et al. Fiber-based generator for wearable electronics and mobile medication. ACS Nano. 2014;**8**:6273-6280

[73] Zhong J, Zhong Q, Hu Q, Wu N, Li W, Wang B. Stretchable self-powered fiber-based strain sensor. Advanced Functional Materials. 2015;**25**:1798-1803